3D integrated hybrid silicon laser

Bowen Song,[1] Cristian Stagarescu,[2] Sasa Ristic,[3] Alex Behfar,[2] and Jonathan Klamkin[1,*]

[1]*Electrical and Computer Engineering Dept., University of California, Santa Barbara, CA, USA*
[2]*M/A-COM Technology Solutions, Ithaca, New York, USA*
[3]*McGill Institute for Advanced Materials, McGill University, Montréal, QC, Canada*
**klamkin@ece.ucsb.edu*

Abstract: Lasers were realized on silicon by flip-chip bonding of indium phosphide (InP) devices containing total internal reflection turning mirrors for surface emission. Light is coupled to the silicon waveguides through surface grating couplers. With this technique, InP lasers were integrated on silicon. Laser cavities were also formed by coupling InP reflective semiconductor optical amplifiers to microring resonator filters and distributed Bragg reflector mirrors. Single-mode continuous wave lasing was demonstrated with a side mode suppression ratio of 30 dB. Up to 2 mW of optical power was coupled to the silicon waveguide. Thermal simulations were also performed to evaluate the low thermal impedance afforded by this architecture and potential for high wall-plug efficiency.

OCIS codes: (250.5300) Photonic integrated circuits; (130.0130) Integrated optics; (140.5960) Semiconductor lasers.

References

1. C. Gunn, "CMOS photonics for high-speed interconnects," IEEE Micro **26**(2), 58–66 (2006).
2. M. Iqbal, M. A. Gleeson, B. Spaugh, F. Tybor, W. G. Gunn, M. Hochberg, T. Baehr-Jones, R. C. Bailey, and L. C. Gunn, "Label-Free Biosensor Arrays Based on Silicon Ring Resonators and High-Speed Optical Scanning Instrumentation," IEEE J. Sel. Top. Quantum Electron. **16**(3), 654–661 (2010).
3. A. Malacarne, F. Gambini, S. Faralli, J. Klamkin, and L. Poti, "High-Speed Silicon Electro-Optic Microring Modulator for Optical Interconnects," IEEE Photonics Technol. Lett. **26**(10), 1042–1044 (2014).
4. F. Morichetti, A. Canciamilla, C. Ferrari, M. Torregiani, A. Melloni, and M. Martinelli, "Roughness Induced Backscattering in Optical Silicon Waveguides," Phys. Rev. Lett. **104**(3), 033902 (2010).
5. H. Zhao, Y. Wang, A. Capretti, L. D. Negro, and J. Klamkin, "Broadband Electroabsorption Modulators Design Based on Epsilon-Near-Zero Indium Tin Oxide," IEEE J. Sel. Top. Quantum Electron. **21**(4), 192–198 (2015).
6. C. R. Doerr, L. Chen, D. Vermeulen, T. Nielsen, S. Azemati, S. Stulz, G. McBrien, X. Xu, B. Mikkelsen, M. Givehchi, C. Rasmussen, and S. Y. Park, "Single-chip silicon photonics 100-Gb/s coherent transceiver," in *Optical Fiber Communication Conference Postdeadline Papers* (Optical Society of America, 2014), paper Th5C.1.
7. J. Klamkin, F. Gambini, S. Faralli, A. Malacarne, G. Meloni, G. Berrettini, G. Contestabile, and L. Potì, "A 100-Gb/s noncoherent silicon receiver for PDM-DBPSK/DQPSK signals," Opt. Express **22**(2), 2150–2158 (2014).
8. C. R. Doerr, L. Chen, and D. Vermeulen, "Silicon photonics broadband modulation-based isolator," Opt. Express **22**(4), 4493–4498 (2014).
9. K. W. Lee, A. Noriki, K. Kiyoyama, T. Fukushima, T. Tanaka, and M. Koyanagi, "Three-Dimensional Hybrid Integration Technology of CMOS, MEMS, and Photonics Circuits for Optoelectronic Heterogeneous Integrated Systems," IEEE Trans. Electron Dev. **58**(3), 748–757 (2011).
10. J. Liu, X. Sun, R. Camacho-Aguilera, L. C. Kimerling, and J. Michel, "Ge-on-Si laser operating at room temperature," Opt. Lett. **35**(5), 679–681 (2010).
11. M. Tang, S. Chen, J. Wu, Q. Jiang, V. G. Dorogan, M. Benamara, Y. I. Mazur, G. J. Salamo, A. Seeds, and H. Liu, "1.3-μm InAs/GaAs quantum-dot lasers monolithically grown on Si substrates using InAlAs/GaAs dislocation filter layers," Opt. Express **22**(10), 11528–11535 (2014).
12. T. Frost, S. Jahangir, E. Stark, S. Deshpande, A. Hazari, C. Zhao, B. S. Ooi, and P. Bhattacharya, "Monolithic Electrically Injected Nanowire Array Edge-Emitting Laser on (001) Silicon," Nano Lett. **14**(8), 4535–4541 (2014).
13. S. Keyvaninia, G. Roelkens, D. Van Thourhout, C. Jany, M. Lamponi, A. Le Liepvre, F. Lelarge, D. Make, G.-H. Duan, D. Bordel, and J.-M. Fedeli, "Demonstration of a heterogeneously integrated III-V/SOI single wavelength tunable laser," Opt. Express **21**(3), 3784–3792 (2013).
14. A. W. Fang, H. Park, O. Cohen, R. Jones, M. J. Paniccia, and J. E. Bowers, "Electrically pumped hybrid AlGaInAs-silicon evanescent laser," Opt. Express **14**(20), 9203–9210 (2006).
15. D. Liang and J. E. Bowers, "Recent progress in lasers on silicon," Nat. Photonics **4**(8), 511–517 (2011).

#260928 Received 15 Mar 2016; revised 27 Apr 2016; accepted 2 May 2016; published 4 May 2016

16. G.-H. Duan, C. Jany, A. Leliepvre, A. Accard, M. Lamponi, D. Make, P. Kaspar, G. Levaufre, N. Girard, F. Lelarge, J.-M. Fedeli, A. Descos, B. Ben Bakir, S. Messaoudene, D. Bordel, S. Menezo, G. de Valicourt, S. Keyvaninia, G. Roelkens, D. V. Thourhout, D. J. Thomson, F. Y. Gardes, and G. T. Reed, "Hybrid III-V on Silicon Lasers for Photonic Integrated Circuits on Silicon," IEEE J. Sel. Top. Quantum Electron. **20**(4), 158 (2014).
17. E. Marchena, T. Creazzo, S. B. Krasulick, P. Yu, D. Van Orden, J. Y. Spann, C. C. Blivin, J. M. Dallesasse, P. Varangis, R. J. Stone, and A. Mizrahi, "Integrated Tunable CMOS Laser for Si Photonics," *Optical Fiber Communication Conference/National Fiber Optic Engineers Conference*, OSA Technical Digest (online) (Optical Society of America, 2013), paper PDP5C.7.
18. N. Kobayashi, K. Sato, M. Namiwaka, K. Yamamoto, S. Watanabe, T. Kita, H. Yamada, and H. Yamazaki, "Silicon Photonic Hybrid Ring-Filter External Cavity Wavelength Tunable Lasers," J. Lightwave Technol. **33**(6), 1241–1246 (2015).
19. N. Hatori, T. Shimizu, M. Okano, M. Ishizaka, T. Yamamoto, Y. Urino, M. Mori, T. Nakamura, and Y. Arakawa, "A Hybrid Integrated Light Source on a Silicon Platform Using a Trident Spot-Size Converter," J. Lightwave Technol. **32**(7), 1329–1336 (2014).
20. D. Feng, J. Luff, S. Jatar, and M. Asghari, "Micron-scale Silicon Photonic Devices and Circuits," in *Optical Fiber Communication Conference*, OSA Technical Digest (online) (Optical Society of America, 2014), paper Th4C.1.
21. P. Contu, C. Stagarescu, A. Behfar, and J. Klamkin, "3D integrated silicon photonic external cavity laser (SPECL)," in *Proceedings of IEEE Photonics Conference*, (2014), pp. 258–259.
22. B. Song, P. Contu, C. Stagarescu, S. Pinna, P. Abolghasem, S. Ristic, N. Bickel, J. Bowker, A. Behfar, and J. Klamkin, "3D integrated hybrid silicon laser," in *European Conference on Optical Communications*, (2015), paper We2.5.5.
23. M. Antelius, K. B. Gylfason, and H. Sohlström, "An apodized SOI waveguide-to-fiber surface grating coupler for single lithography silicon photonics," Opt. Express **19**(4), 3592–3598 (2011).
24. G. Roelkens, D. Van Thourhout, and R. Baets, "High efficiency Silicon-on-Insulator grating coupler based on a poly-Silicon overlay," Opt. Express **14**(24), 11622–11630 (2006).
25. Y. Li, L. Li, B. Tian, G. Roelkens, and R. G. Baets, "Reflectionless Tilted Grating Couplers With Improved Coupling Efficiency Based on a Silicon Overlay," IEEE Photonics Technol. Lett. **25**(13), 1195–1198 (2013).
26. A. Khanna, Y. Drissi, P. Dumon, R. Baets, P. Absil, J. Pozo, D. M. R. Lo Cascio, M. Fournier, J.-M. Fédéli, L. Fulbert, L. Zimmermann, B. Tillack, T. Aalto, P. O'Brien, D. Deptuck, J. Xu, and D. Gale, "Epixfab: the silicon photonics platform," Proc. SPIE **8767**, 87670H (2013).
27. A. Behfar, A. Schremer, M. Green, C. Stagarescu, and A. Morrow, "Horizontal cavity surface-emitting laser (HCSEL) Devices," Proc. SPIE **5737**, 62–69 (2005).

1. Introduction

Among all platforms available to implement photonic integrated circuits (PICs), silicon photonics (SiPh) has emerged as perhaps the most attractive, especially for communications and switching applications in high performance computers and data centers [1]. SiPh is also expected to impact other areas including telecommunications, sensing, free space optics, and biomedicine [2]. SiPh utilizes CMOS-compatible processes, which are capable of producing devices and integrated circuits at low cost and in high volumes. The high index contrast waveguide platform characteristic of silicon on insulator (SOI), used for SiPh, also enables small footprint and other attractive properties for novel devices [3–5].

Although SiPh has undergone significant maturation in recent years [6–8], the integration of low cost and high efficiency laser sources still remains an open problem. SiPh interposer technologies also require the integration of PICs realized in other platforms such as indium phosphide (InP) [9]. For such integration, high coupling efficiency is critical. Monolithic integration techniques based on heteroepitaxy have been proposed for lasers. These include germanium on silicon, quantum dots on silicon, and nanowire lasers [10–12]. These approaches are promising for future large-scale photonic integration, but are immature. Only discrete lasers on silicon have been realized with these approaches thus far.

The heterogeneous integration of III-V semiconductors using wafer bonding techniques has demonstrated a host of novel active PICs on silicon [13–16]. With this approach, sensitive wafer bonding steps are required to combine III-V materials (typically InP) with silicon. This approach requires co-fabrication of InP and silicon, which are incompatible materials. Also, the InP gain material is bonded to the SOI layer, therefore the gain medium is thermally isolated from the substrate by the buried oxide (BOX). Lasers realized with this approach exhibit high thermal impedance limiting their efficiency and potential for high temperature operation, the latter of which is critical for on-chip applications. InP and silicon also exhibit different coefficients of thermal expansion, therefore, reliability is a concern for devices

#260928 Received 15 Mar 2016; revised 27 Apr 2016; accepted 2 May 2016; published 4 May 2016

realized by direct wafer bonding. Hybrid integration technology, which involves butt coupling to silicon waveguides, has also been demonstrated. However, direct coupling to silicon nanowires is challenging due to the significant mode mismatch of the waveguides thereby requiring intermediate coupling elements [17–19]. Since typical InP lasers exhibit large divergence, precise alignment is required in all dimensions, especially the vertical dimension. Although large silicon waveguides can alleviate the mode mismatch issue [20], such waveguides are not conducive to sharp bend radii, which is a principal benefit of SiPh.

We previously proposed a novel 3D integration technique for realizing lasers on silicon [21]. This hybrid approach is based on flip-chip bonding of an InP laser or gain chip to a SiPh chip. The InP chip contains a monolithic total internal reflection (TIR) turning mirror for vertical emission [22]. Based on this 3D integration technique, we also proposed a silicon photonic external cavity laser (SPECL) comprising an InP gain element coupled to silicon feedback and filter elements. Compared to other laser integration approaches, 3D integration has many advantages. The InP chip can be flip-chip bonded P-side (epi-side) down to the silicon substrate. This allows for efficient heat removal from the active gain medium. Thermal simulations show that lasers realized in this way with 3D integration demonstrate low thermal impedance, which facilitates high laser efficiency and high temperature operation. Integration with standard 220-nm SOI is also possible, whereas other approaches generally require a thicker silicon waveguide layer. Since the InP and silicon frontend processes are carried out separately, the 3D integration technique does not require co-fabrication of these materials. The attachment of InP chips, which is carried out in a backend step, is accomplished with a standard flip-chip bonding technique that has been widely used in the integrated circuit industry. Furthermore, the metal used for bonding can alleviate thermal expansion coefficient mismatch. The integration can also be carried out at wafer level meaning that InP chips can be attached within die on a full SiPh wafer. The 3D integration approach is highly scalable in that increasing the number of lasers integrated can be enabled by increasing the InP chip size, by more densely packing the number of lasers within the InP chip, or by bonding more InP chips.

Here we report on the demonstration and analysis of an integrated hybrid silicon laser based on 3D integration. Single mode continuous wave lasing was demonstrated with a threshold current of 23 mA at a temperature of 20°C. At a current level of 100 mA, a maximum optical power coupled into the silicon waveguide of 2 mW was achieved. With a distributed Bragg reflector (DBR) mirror and microring resonator filter, both fabricated in the SOI for forming a laser cavity, a side-mode suppression ratio (SMSR) of 30 dB was measured. Thermal simulations are also reported illustrating the benefits of bonding directly to the silicon substrate, which is possible with 3D integration. Although the devices fabricated here emit near the 1550-nm wavelength regime, the concepts translate directly to the 1310-nm regime as well. The latter is applicable to short-reach applications such as data communications.

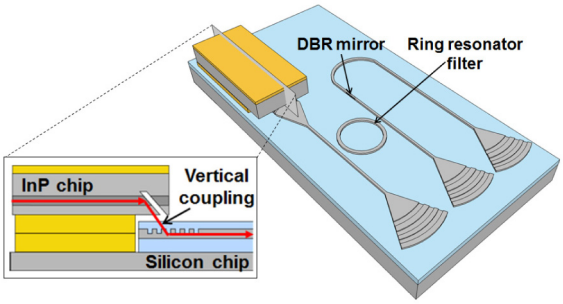

Fig. 1. Schematic of 3D integrated hybrid silicon laser.

#260928 Received 15 Mar 2016; revised 27 Apr 2016; accepted 2 May 2016; published 4 May 2016

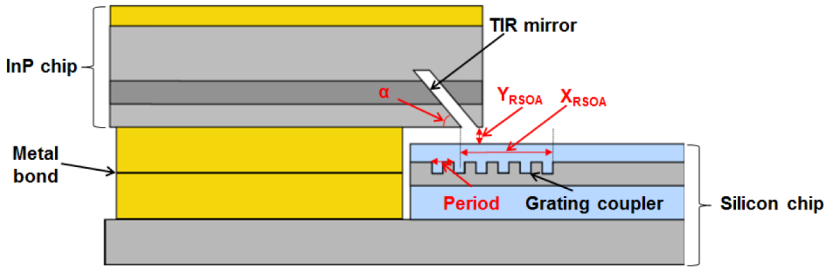

Fig. 2. Sideview schematic illustrating design details for 3D integration with vertical coupling.

2. 3D integration and vertical coupling simulations

The 3D integration technique can be used to integrate lasers or PICs on silicon. The focus of this report is the integration of reflective semiconductor optical amplifiers (RSOAs) and the design and realization of SPECLs that contain RSOAs. A schematic of the 3D hybrid SPECL is shown in Fig. 1. The RSOA contains a high reflectivity (HR) coated back mirror and a TIR turning mirror. The hybrid laser cavity consists of the RSOA, a grating coupler, a ring resonator filter, and a distributed Bragg reflector (DBR) mirror. The DBR mirror provides filtered feedback for the laser, and the ring resonator provides additional filtering for narrowband lasing. In this work, we demonstrate lasers both with and without the additional ring resonator filter. Without the additional filter, the device behaves as a DBR laser.

A sideview illustration of the 3D integrated coupling structure is shown in Fig. 2 with the parameters used for coupling optimization highlighted in red. The RSOA structure consists of an indium gallium arsenide phosphide active waveguide with InP cladding layers. An anti-reflection (AR) coating was applied to the emitting surface of the RSOA to reduce reflections. The TIR turning mirror angle was optimized for high coupling efficiency to the silicon waveguide. The SOI waveguide layer is 220 nm thick and the BOX layer is 2 μm thick. In the grating coupler region, the silicon is 380 nm thick and the etch depth of the grating is 220 nm.

The mode evolution and coupling are shown in Fig. 3. The light propagating in the RSOA waveguide is redirected vertically by the turning mirror. The light then exits the InP chip and eventually couples into the silicon waveguide through the grating coupler. The grating coupler design should be optimized for the expected incident mode. In comparison to a fiber mode, this waveguide mode is likely smaller and more divergent, although advanced waveguide designs can be utilized to minimize the divergence.

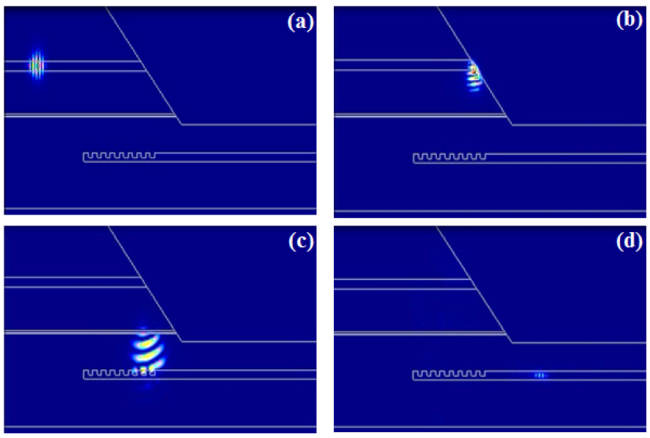

Fig. 3. Mode evolution and coupling. (a) Optical pulse propagating in the InP waveguide. (b) Total internal reflection at the turning mirror. (c) Light exiting the InP chip and propagating toward the silicon chip. (d) Coupling into the silicon waveguide through the surface grating.

#260928 Received 15 Mar 2016; revised 27 Apr 2016; accepted 2 May 2016; published 4 May 2016

High coupling efficiency silicon grating couplers have been demonstrated in [22] and [24]. These grating couplers were primarily optimized for fiber coupling. In order to maximize the coupling efficiency from the RSOA to the silicon waveguide, 2D and 3D finite difference time domain (FDTD) simulations were performed. The RSOA devices used in experiments utilize a fairly conventional waveguide design, similar to that used for commercial diode lasers. The waveguide mode is small, asymmetric, and fairly divergent. Using 2D simulations initially, a number of parameters were optimized including the grating period, the grating fill factor, the turning mirror angle (α), and the horizontal and vertical positon of the RSOA with respect to the silicon grating (X_{RSOA} and Y_{RSOA}). The 2D FDTD simulation results are summarized in Fig. 4. These simulations consider conventional photonic elements illustrating performance for a low-cost approach. Neither the RSOA waveguide nor the silicon waveguide were optimized, and the grating period and fill factor were uniform. As will be shown, significant improvements can be made by incorporating other concepts such as grating apodization and optimized waveguide designs. Nevertheless, these initial 2D simulations provided a starting point for the design and validated some of the results, which are described in detail in the following section. The simulations also provide some insight into the tolerances of this low-cost and non-optimized approach. For example, Fig. 4(c) shows that the coupling efficiency is not extremely sensitive to the turning mirror angle; at a wavelength 1550 nm, a change of 2 degrees in the mirror angle will yield a reduction in coupling efficiency of less than 5%. Also, referring to Fig. 4(d), it can be observed that alignment inaccuracies on the order of 1 μm do not significantly degrade the coupling.

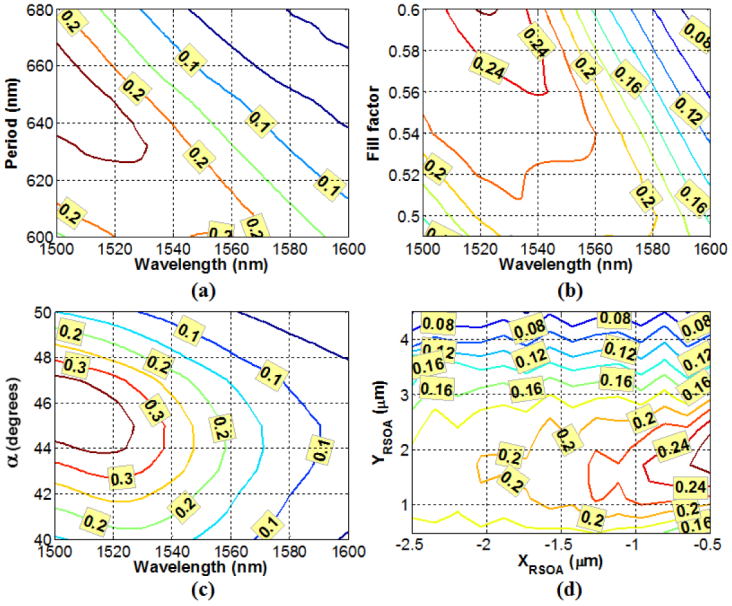

Fig. 4. Coupling efficiency as a function of (a) wavelength and grating period (for fill factor = 0.6, α = 48°, Y_{RSOA} = 2 μm, X_{RSOA} = –0.5 μm), (b) wavelength and fill factor (for period = 635 nm, α = 48°, Y_{RSOA} = 2 μm, X_{RSOA} = –0.5 μm), (c) wavelength and turning mirror angle (for period = 635 nm, fill factor = 0.6, Y_{RSOA} = 2 μm, X_{RSOA} = –0.5 μm), (d) horizontal and vertical position of the RSOA with respect to the grating (X_{RSOA} and Y_{RSOA}) (for period = 635 nm, fill factor = 0.6, α = 48°).

Based on the 2D optimization, 3D FDTD simulations were then performed. To evaluate the vertical coupling 3D integration technique, several attributes were investigated including the silicon waveguide thickness, the grating design type, the design of the taper for transitioning from the wide grating region to a single mode waveguide, as well as other elements including the design of the RSOA waveguide and inclusion of a lower (below the silicon waveguide) reflector. Table 1 summarizes the designs that were explored and Fig. 5

#260928 Received 15 Mar 2016; revised 27 Apr 2016; accepted 2 May 2016; published 4 May 2016

shows the corresponding 3D simulated coupling efficiency spectra for these designs. Although the results from the 2D simulations were used as a starting point, all design attributes were optimized for each design reported in Fig. 5. Included in the 3D simulations is the design of the grating illumination area and curvature of the gratings, the latter for assisting with the lateral taper that transitions from a wide waveguide to a narrow single mode nanowire waveguide. Design 3 represents the attributes used in the 2D simulations. For this design, the silicon thickness in the grating region was 380 nm, the grating period and fill factor were uniform (grating period = 635 nm, fill factor = 0.6), and, specifically for 3D simulations, the grating illumination area and grating curvature were optimized for the mode incident from the RSOA.

Design 1 represents that which was used for the experiments detailed in the following sections. The main shortcomings of this design are that the grating coupler, specifically the grating illumination area and curvature, were optimized for fiber coupling and not for coupling from a RSOA. Although this provided a means for experimental demonstration, the coupling efficiency was low thereby limiting the overall performance. Significant improvements can be made as described by the other designs reported in Fig. 5. Design 4, for example, incorporates an optimized silicon waveguide thickness, a uniform grating (grating period = 615 nm, fill factor = 0.5) that was optimized for coupling from the RSOA, and a RSOA with a dilute waveguide. The dilute waveguide was designed to emit a beam that is larger in size and characteristic of low angular divergence. Since the mode size is larger, the corresponding grating coupler includes more grating periods for illumination. Therefore, the coupling bandwidth is slightly narrower. This design can achieve a coupling efficiency of 50%, which is as good as many of the other laser integration techniques reported elsewhere. To improve the performance further, Design 5 includes a lower reflector and a grating with period and fill factor identical to those used in Design 4. This reflector is placed an optimized distance below the silicon waveguide and increases the coupling efficiency to approximately 75%. Design 6 incorporates an apodized grating [23] with period and fill factor for each grating period as follows (period/fill factor): 604 nm/0.37, 594 nm/0.32, 586 nm/0.28, 580 nm/0.25, 574 nm/0.22, 570 nm/0.2, 564 nm/0.17, 560 nm/0.15, 556 nm/0.13, 550 nm/0.1, 548 nm/0.08. This design increases the coupling efficiency to 85%, which, to our knowledge, would represent the highest coupling efficiency for any silicon laser integration approach. Future designs could also incorporate reflectionless grating couplers to manage reflections at the grating coupler interface [25]. In summary, the designs described in Fig. 5 illustrate different levels of performance and complexity that could be realized using the 3D vertical coupling integration approach.

Table 1. Grating Coupler Designs

Design	Silicon thickness	Grating design	Silicon waveguide lateral taper	Additional elements
(1)	380 nm	Uniform	Optimized for fiber	-
(2)	220 nm	Uniform	Optimized for RSOA	-
(3)	380 nm	Uniform	Optimized for RSOA	-
(4)	520 nm	Uniform	Optimized for RSOA	Dilute RSOA waveguide
(5)	520 nm	Uniform	Optimized for RSOA	Dilute RSOA waveguide, lower reflector
(6)	520 nm	Apodized	Optimized for RSOA	Dilute RSOA waveguide, lower reflector

#260928 Received 15 Mar 2016; revised 27 Apr 2016; accepted 2 May 2016; published 4 May 2016

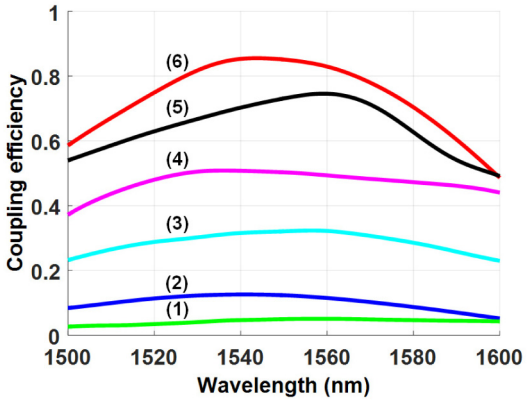

Fig. 5. 3D FDTD simulation results showing the coupling efficiency as a function of wavelength for baseline.

3. Device fabrication and bonding

The silicon chips were fabricated at the Interuniversity Microelectronics Centre (IMEC) from 200-mm SOI wafers [26]. The thickness of the silicon waveguide layer is 220 nm. The poly-silicon overlay and patterning was incorporated to increase the silicon thickness to 380 nm in the grating regions. The DBR mirrors were realized with edge-corrugated gratings. The reflectivity and 3-dB bandwidth of the DBR mirrors are approximately 40% and 10 nm, respectively. The ring resonator has a free spectral range and a quality factor of approximately 19 nm and 1000, respectively. The waveguide loss is approximately 2 dB/cm and the bend loss for the rings is negligible. The fabrication process also includes germanium deposition for the realization of photodetectors and ion implantation steps for the formation of P-N junctions. High-speed Mach-Zehnder modulators (MZMs) and germanium photodetectors were realized on the chips. The MZMs could be used for realizing transmitters. The germanium photodetectors were used primarily for calibrating fiber coupling loss.

The InP RSOAs were fabricated with an etched-facet process that is conducive to low-cost manufacturing [27]. Both the back facet and the turning mirror were formed by chemically-assisted ion beam etching. An HR coating was applied to the back facet and an AR coating was applied to the exit surface of the surface emitting device. P-metal contacts were formed on the topside and N-metal contacts on the backside. InP chips with four RSOAs were singulated following on-wafer testing and coating. These chips are approximately 1.5 x 1.0 mm^2. The lateral spacing of the RSOAs was made conservatively large. Therefore, more RSOAs could be incorporated in a chip of this size, or a smaller chip could be realized containing four RSOAs. For the SPECLs characterized and reported here, the RSOA gain length, L_{Gain}, was 1 mm.

Thermo-compression bonding was used to attach the InP RSOAs to the silicon chips. The RSOA chips were bonded P-side down. The flip-chip bonding tool utilized is capable of 1-µm alignment accuracy. Both chips were cleaned using solvents before bonding. The bonding temperature was 350°C and the force applied was approximately 20 N. A topview microscope image of a 3D integrated laser structure is shown in Fig. 6(a). Figure 6(b) shows a tilted planview of a bonded InP RSOA chip and Fig. 6(c) shows a close up of the bonded chips.

#260928 Received 15 Mar 2016; revised 27 Apr 2016; accepted 2 May 2016; published 4 May 2016

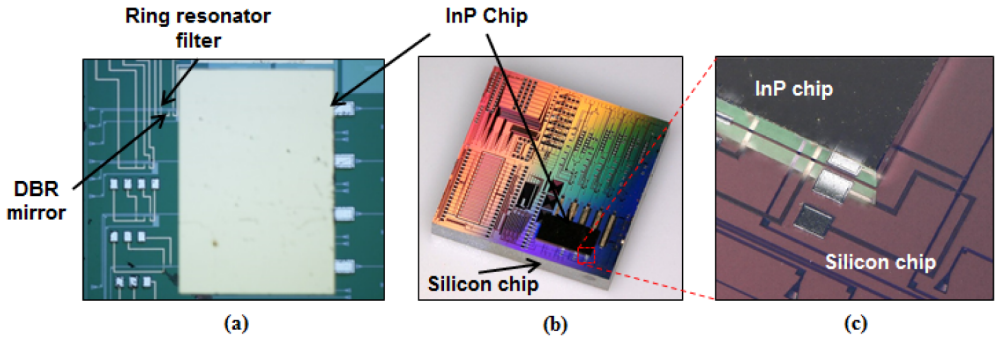

Fig. 6. (a) Topview microscope image of a 3D integrated hybrid laser. (b) Tilted planview image of a bonded RSOA chip on silicon. (c) Close up of bonded chips.

To evaluate the electrical quality of the metal bond, the current-voltage (IV) characteristics were measured both for a standalone InP RSOA and for a 3D integrated laser. The gain length was identical for both devices (1 mm). As shown in Fig. 7, the IV characteristics are nearly identical indicating that the metal bond makes a proper electrical connection and does not introduce additional resistance.

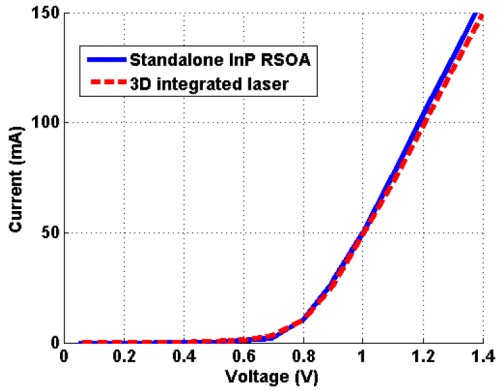

Fig. 7. IV characteristics for 3D integrated laser and standalone InP RSOA.

4. Laser experimental results

To evaluate the laser performance experimentally, the 3D integrated laser was mounted to a temperature-controlled stage and electrically pumped using pin probes. A vertically oriented single mode fiber probe was used to collect light from the output of the SPECL through a fiber grating coupler. Spectral measurements were made with an optical spectrum analyzer having a resolution of 0.02 nm. Figure 8(a) shows the lasing spectra at different current levels near threshold. At 20°C, single-mode continuous wave lasing was observed with a threshold current of 23 mA. The light-current-voltage (LIV) characteristic is shown in Fig. 8(b). At a current level of 100 mA, the optical power coupled in the silicon waveguide was 2 mW.

SPECLs both with and without the intracavity microring resonator filter were characterized and compared. Figure 9 shows the single mode output spectra of these SPECLs. For the SPECL with a microring filter, the center wavelength was measured to be 1557.5 nm and the peak optical power was 0.5 mW at a current of 48 mA. The SMSR was measured to be greater than 30 dB. For the SPECL without the microring filter (DBR mirror only), the lasing wavelength was measured to be 1562.5 nm. The optical output power was 1.4 mW at a RSOA current of 72.8 mA and the SMSR was measured to be 30 dB.

#260928 Received 15 Mar 2016; revised 27 Apr 2016; accepted 2 May 2016; published 4 May 2016

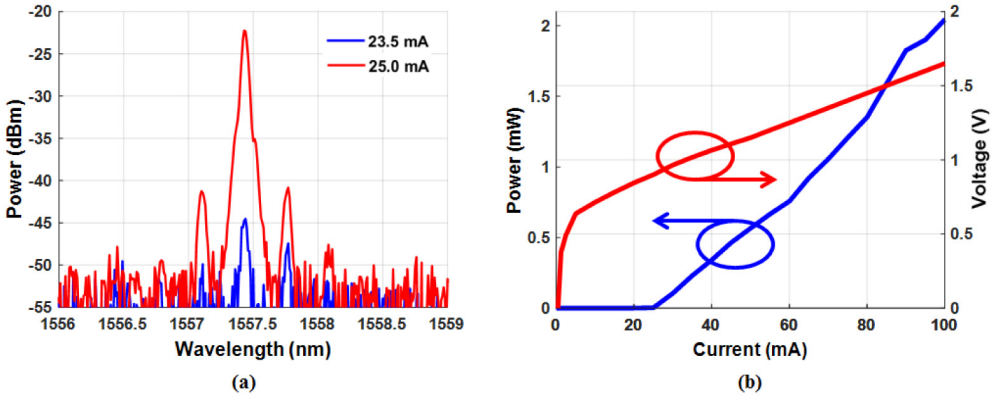

Fig. 8. (a) Lasing spectra at two different current levels near threshold and (b) LIV characteristic for for the 3D integrated laser with microring resonator filter and DBR mirror.

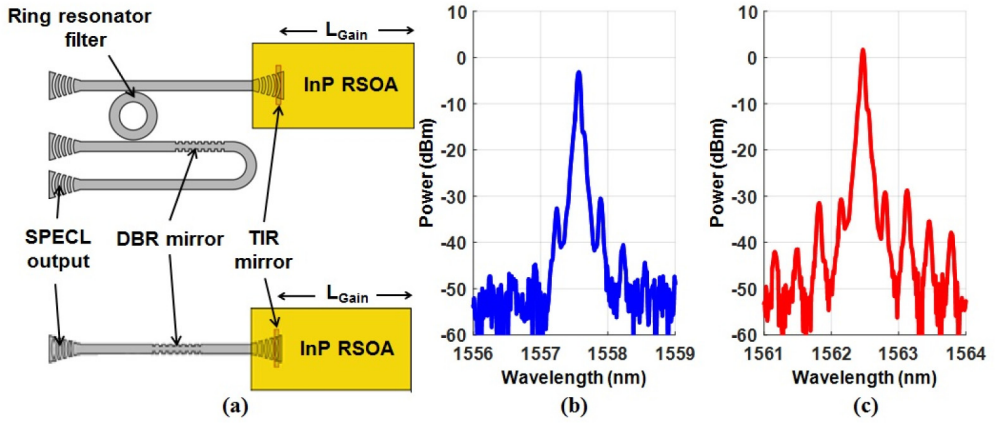

Fig. 9. (a) Topview schematic of SPECL with microring filter (top) and without microring filter (bottom). Spectrum of SPECL (b) with microring filter and (c) without microring filter.

4. Thermal performance analysis

The 3D hybrid integration technology allows for the InP active chips to be bonded P-side down directly to the silicon substrate, providing an effective means to dissipate heat generated in the gain medium. Other laser integration approaches do not necessarily allow for this type of arrangement. With the wafer bonding approach, for example, the active gain medium is physically separated from the silicon substrate by the BOX layer. Heat generated in the gain medium is trapped with this approach leading to poor thermal performance. To quantify the advantage afforded by the 3D integration approach, finite element method simulations were performed and the results are presented in Fig. 10. A thermal profile for an InP active structure bonded to a silicon dioxide (SiO_2) layer is shown in Fig. 10(a) and that for an InP active structure bonded directly to a silicon substrate is shown in Fig. 10(b). The former is representative of what would be observed for the wafer bonding approach. For the structure with the SiO_2, which thermally isolates the InP from the silicon substrate, a thermal impedance·length product of 3.7×10^{-2} Km/W was extracted from the simulations. Expressing the thermal impedance this way allows for comparison to laser structures reported elsewhere that may have different lengths. For the structure bonded directly to the silicon substrate, the thermal impedance·length was extracted to be 1.5×10^{-2} Km/W. The thermal impedance for a laser realized with the 3D integration technique, where the laser is bonded directly to the

#260928 Received 15 Mar 2016; revised 27 Apr 2016; accepted 2 May 2016; published 4 May 2016

silicon substrate, is therefore a factor of 2.5 lower than that of a structure with SiO_2 forming a thermal barrier. Lasers realized with 3D integration can therefore operate more efficiently and at higher temperatures.

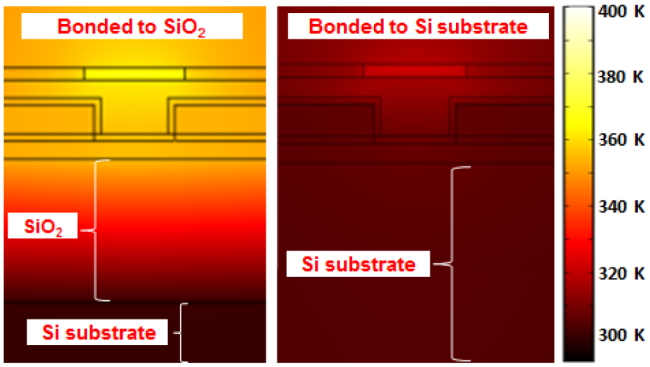

Fig. 10. Simulated thermal profile for (a) InP active structure bonded to a SiO_2 layer on a silicon substrate and for (b) InP active structure bonded directly to silicon substrate.

5. Conclusion

A novel 3D integrated hybrid silicon laser was experimentally demonstrated and analyzed. The laser was constructed by flip-chip bonding an InP RSOA with a TIR turning mirror to a SiPh chip with a surface grating coupler. Up to 2 mW of optical power was coupled to the silicon waveguide using this approach. Single mode CW lasing was also observed with an SMSR of 30 dB for SPECL structures both with and without an intracavity microring resonator filter. Finally, thermal simulations demonstrated drastic reduction in thermal impedance when bonding an InP active medium directly to the silicon substrate. The 3D hybrid silicon laser has many advantages over other SiPh laser approaches and could enable large-scale integration.

Acknowledgments

The authors acknowledge NASA for support through the Early Career Faculty Space Technology Research Grant. The authors also acknowledge Sergio Pinna, Pietro Contu, and Warren Jin for assistance with design and simulations, and Payam Abolghasem, Nathan Bickel, and Jason Bowker for RSOA fabrication and characterization.

#260928 Received 15 Mar 2016; revised 27 Apr 2016; accepted 2 May 2016; published 4 May 2016